b-value of what? Complex behavior of the magnitude distribution during and within the 2016–2017 central Italy sequence

Marcus Herrmann (marcus.herrmann@unina.it)
Università degli Studi di Napoli 'Federico II' https://orcid.org/0000-0002-2342-1970
Ester Piegari
Università degli Studi di Napoli 'Federico II'
Warner Marzocchi
University of Naples, Federico II https://orcid.org/0000-0002-9114-1516

Article

Keywords:

Posted Date: January 7th, 2022

DOI: https://doi.org/10.21203/rs.3.rs-1210699/v1

Version of Record: A version of this preprint was published at Nature Communications on August 29th, 2022. See the published version at https://doi.org/10.1038/s41467-022-32755-6.

b-value of what? Complex behavior of the magnitude distribution during and within the 2016–2017 central Italy sequence

Marcus Herrmann*[1], Ester Piegari[1], Warner Marzocchi[1]

[1] Dipartimento di Scienze della Terra, dell'Ambiente e delle Risorse; Università degli Studi di Napoli 'Federico II', Naples, Italy

* Corresponding author: marcus.herrmann@unina.it

December 28, 2021

Abstract:

The Magnitude–Frequency-Distribution (MFD) of earthquakes is typically modeled with the (tapered) Gutenberg–Richter relation. The main parameter of this relation, the b-value, controls the relative rate of small and large earthquakes. Resolving spatiotemporal variations of the b-value is critical to understanding the earthquake occurrence process and improving earthquake forecasting. However, this variation is not well understood. Here we present unexpected MFD variability using a high-resolution earthquake catalog of the 2016–2017 central Italy sequence. Isolation of seismicity clusters reveals that the MFD differs in nearby clusters, varies or remains constant in time depending on the cluster, and features an unexpected b-value increase in the cluster where the largest event will occur. These findings suggest a strong influence of the heterogeneity and complexity of tectonic structures on the MFD. Our findings raise the question of the appropriate spatiotemporal scale for resolving the b-value, which poses a serious obstacle to interpreting and using the MFD in earthquake forecasting.

1 Introduction

Beroza et al. [2021] recently highlighted that current earthquake catalogs achieve a high level of detail that likely contains more information about earthquake occurrence, allows testing of existing hypotheses, and potentially improves earthquake forecasting. One of the main ingredients for earthquake forecasting and seismic hazard models is the Magnitude–Frequency-Distribution (MFD) of earthquakes, which carries information about the proportion between small and large earthquakes. The MFD is typically modeled with the Gutenberg–Richter (GR) relation and its b-value (the slope of the GR relation), which can be used to infer the occurrence rate of large earthquakes from small ones. The b-value is observed to vary in space and time [e. g., *Wiemer and Wyss* 1997; *Hainzl and Fischer* 2002; *Tormann et al.* 2013; *Gulia et al.* 2016; *Shelly et al.* 2016; *Petruccelli et al.* 2019; *Taroni et al.* 2021], which is thought to be primarily related to variations of the stress state in the crust [e. g., *Wyss* 1973; *Scholz* 2015; *El-Isa and Eaton* 2014]. The b-value is also considered as an indicator for other conditions in the crust, which are directly or indirectly related to the stress state, such as faulting style [e. g., *Schorlemmer et al.* 2005; *Petruccelli et al.* 2019], locked or creeping fault patches [e. g., *Wiemer and Wyss* 1997; *Sobiesiak et al.* 2007; *Ghosh et al.* 2008; *Tormann et al.* 2013], material properties [e. g., *Mogi* 1962; *Goebel et al.* 2017], fluid pore-pressure perturbations [e. g., *Hainzl and Fischer* 2002; *Bachmann et al.* 2012; *Shelly et al.* 2016; *Passarelli et al.* 2015], and critical nucleation length [*Dublanchet* 2020], among others [see *El-Isa and Eaton* 2014, and references therein]. b-value variations may therefore have an important role in improving our physical understanding of earthquake occurrence.

Estimating the b-value appears trivial in theory (after all, it is simply the rate parameter of an exponential distribution), but not in practice. Several aspects affect the ability to resolve representative b-value variations in earthquake catalogs, such as:

1. the quality of the data, its spatiotemporal selection, and the various ways of sampling it [e. g., *Tormann et al.* 2013; *Roberts et al.* 2016];
2. the sample size and available magnitude range [e. g., *Wiemer and Wyss* 2002; *Marzocchi and Sandri* 2003; *Roberts et al.* 2016; *Nava et al.* 2016];
3. the used magnitude scale, magnitude binning, and maximum likelihood estimator [*Wiemer and Wyss* 2002; *Marzocchi and Sandri* 2003; *Marzocchi et al.* 2020; *Herrmann and Marzocchi* 2021];
4. the treatment of departures from an exponential-like GR distribution at the upper end (due to truncation or tapering) and lower end (due to the inherent and potentially varying incompleteness) [*Kagan* 2002; *Spassiani and Marzocchi* 2021; *Marzocchi et al.* 2020; *Herrmann and Marzocchi* 2021], e. g., the estimation of the magnitude of completeness, M_c, as the lower magnitude threshold.

Although this list is not exhaustive, these considerations highlight that the outcome of a b-value analysis highly depends on expert judgment and/or subjective choices. A recent scientific discussion between *Gulia and Wiemer* [2021] and *Dascher-Cousineau et al.* [2021] reemphasized that choices have to be specific, meaningful, and reproducible to obtain robust results that contribute to a better understanding of the underlying physical processes. It appears that this field of study requires well-defined schemes and analysis steps. Moreover, choices are critical for real-time applications

that need to run automatically, e. g., for operational earthquake forecasting (OEF) purposes [*Jordan et al.* 2011]. Assessing the influence of expert choices and various modeling ideas on the forecasting performance needs community efforts such as the *Collaboratory for the Study of Earthquake Predictability* (CSEP) [*Zechar et al.* 2010; *Schorlemmer et al.* 2018], which tests forecasting models prospectively in a controlled environment.

Here we argue that a complex earthquake sequence with multiple ruptured fault segments can further bias MFD and b-value analysis: If the MFD varies temporally among tectonic structures, an averaged view over the whole sequence or a smoothed view over a finite scale (either in space or time) will neglect or mask those variations and may lead to inappropriate or biased inferences. Instead, an MFD analysis may become more physically meaningful and less ambiguous when accounting for the internal structure and evolution of a sequence. *Igonin et al.* [2018] already showed that the MFD can significantly differ in adjacent but well-defined zones of induced seismicity. In this study, we introduce a new perspective to investigate the spatiotemporal behavior of the MFD and b-value by isolating spatial seismicity clusters of a complex sequence and dividing them into temporal periods. To define clusters, we use the hypocenter density of a seismic sequence; the temporal periods are defined by occurrence time of the largest events.

We use the 2016–2017 central Italy (hereafter 'CI2016') sequence as an example due to its complex tectonic structure, cascading evolution, and the availability of high-resolution catalogs. The CI2016 sequence occurred in the central Apennines, one of Italy's most seismically active areas, and was marked by a cascade of three main events: the $M_\mathrm{w}6.0$ ($M_\mathrm{L}6.0$) Amatrice event on 24 August 2016, the $M_\mathrm{w}5.9$ ($M_\mathrm{L}5.8$) Visso event on 26 October 2016, and the $M_\mathrm{w}6.5$ ($M_\mathrm{L}6.1$) Norcia mainshock on 30 October 2016. On 18 January 2017, four $M_\mathrm{w}5.0$–5.5 events followed near Campotosto. These seven events have been caused by movements on SW-dipping normal faults and they ruptured multiple fault segments, activating a complex fault system [e. g., *Chiaraluce et al.* 2017; *Improta et al.* 2019; *Michele et al.* 2020; *Porreca et al.* 2020; *Tondi et al.* 2020; *Waldhauser et al.* 2021].

The CI2016 sequence is particular in that it features seismicity in a ∼1 km-thick subhorizontal detachment at around 10 km depth, which intersects with and confines almost the entire normal fault system above [e. g., *Michele et al.* 2016; *Chiaraluce et al.* 2017; *Vuan et al.* 2017; *Michele et al.* 2020; *Waldhauser et al.* 2021]. Such a feature was already observed in the Apennines at a depth of 15–20 km [*De Luca et al.* 2009], which suggested the presence of a buried subhorizontal thrust related to (the deepest part of) the Apennines build-up. It generally appears as a flat layer, and high-resolution catalogs resolved it as a slightly east-dipping, irregular structure (i. e., with locally varying depth and thickness) [*Chiaraluce et al.* 2017]. *Vuan et al.* [2017] interpreted this feature as a midcrustal shear zone, which decouples the upper and lower crust. They found prior seismicity mostly to occur along this structure, suggesting that it was loaded tectonically and eventually favored the unlocking of the shallower faults through stress transfer. *Waldhauser et al.* [2021] identified partially overlapping fault fragments in this structure.

Magnitude statistics of CI2016 have been investigated in several recent studies. *Montuori et al.* [2016] found that the Amatrice event originated in an area with a high b-value and subsequently reduced the b-value to the north and south, suggesting a high potential for further large events. *Gulia and Wiemer* [2019] found a b-value variation during the course of the sequence, in particular (i) a drop after the Amatrice event (especially in the area to the north where the Norcia mainshock occurred afterward), interpreted as a still impending large earthquake, and (ii) a b-value increase

after the Norcia mainshock, interpreted as a substantially reduced chance for a further large event similar to the tectonic background rate. *García-Hernández et al.* [2021] also observed a "marked drop of the b-value" after the Amatrice event (resolved spatially and in depth) and a recovery of the b-value to the background level after the Norcia mainshock; they exclude that these variations are caused by an increased M_c after the main events.

However, those studies did not (i) use a high-resolution catalog, (ii) account for the complexity of the sequence including its depth-dependent structure, and (iii) resolve what happened in the days before the largest event (Norcia). Using a high-resolution catalog, we investigate whether accounting for the complex sequence in an isolated fashion provide a benefit in resolving the spatiotemporal variation of the MFD and b-value. Rather than solely focusing on b-value estimates, we consider it important to exploit more information from the MFD, e. g., by assessing and comparing its exponential-like part and reporting the b-value stability as function of M_c.

2 Results

2.1 Description of clusters

Using the high-resolution catalog of *Tan et al.* [2021], we spatially isolated the five largest seismicity clusters (Cluster 1–5, hereafter abbreviated with C1, C2, etc.) following the procedure described in Methods. Figure 1 shows that the obtained clusters are not randomly distributed, but instead highlight the complex spatial structure of the sequence. For instance, C1 comprises seismicity in the northern part of the subhorizontal structure, parts of the normal fault (Mt. Vettore) that ruptured during the Norcia mainshock, and this mainshock hypocenter itself. C2 represents seismicity in the southern part of the subhorizontal structure, and C3 captures the shallow northern part of the sequence, including the Visso hypocenter. C4 and C5 relate to small-scale structures. These five clusters correspond to the five largest volumes with high hypocenter density (see Supplementary Fig. S1). The Amatrice event does not belong to any of the main clusters because the area around its hypocenter is devoid of events [see also *Improta et al.* 2019; *Michele et al.* 2020; *Tan et al.* 2021]. The Campotosto events were also not assigned to a main cluster.

Figure 2 shows that each cluster has a distinct temporal activity. For instance, C1 was active throughout the sequence until the Campotosto events; C2 was quiet after the Visso event until the Norcia mainshock while C3 was very active in this period. C4 and C5 were mostly active toward the end of the sequence, along with the other clusters in roughly comparable proportions. Supplementary Fig. S2 and Supplementary Note 1 summarize the cluster statistics in terms of size and ratio for each period, making it more apparent that at least ~50% of the events in each period of the sequence belong to a cluster. Moreover, up to two clusters were dominating each period except for the last period.

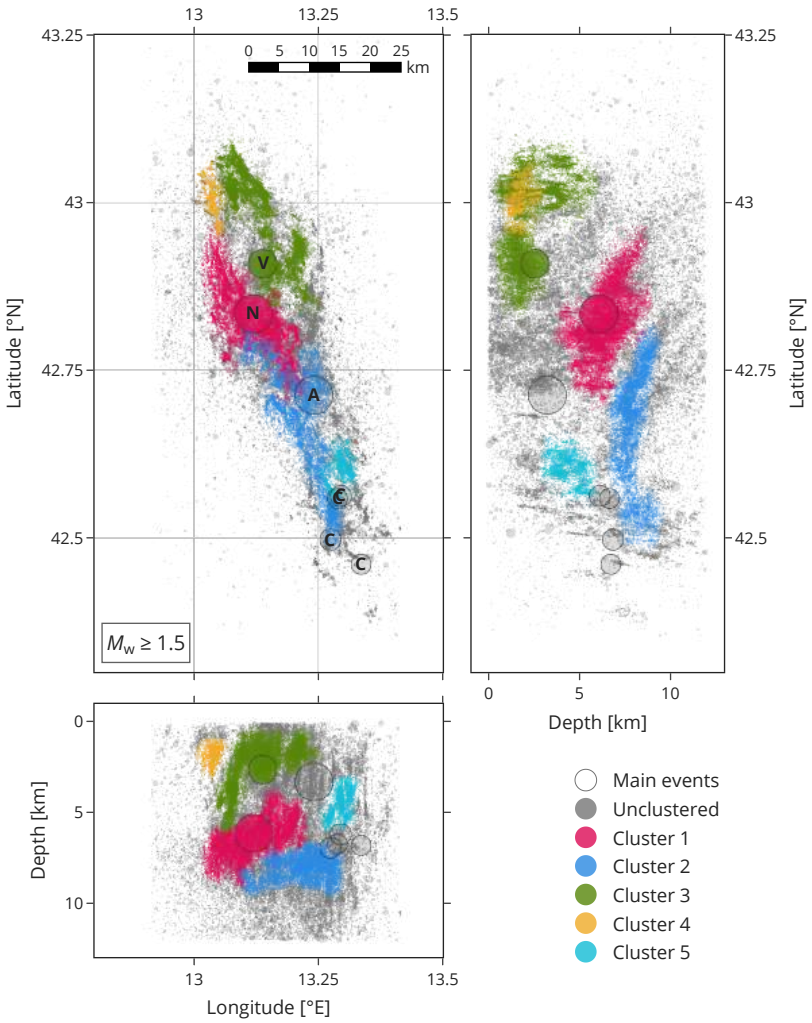

Figure 1: Map view and depth sections of the 2016–2017 central Italy ('CI2016') seismicity with identified clusters (see legend). The depth sections are exaggerated by a factor of three. To better reveal the structure of the individual clusters, the events are plotted ascending by their cluster number on top of 'unclustered' events, neglecting a physically correct appearance. The main events 'Amatrice', 'Visso', 'Norcia', and four 'Campotosto' events are represented by larger circles; in the map view, they are annotated with the respective initial letter (A, V, N, C). Supplementary Fig. S1 shows the event density for the same data.

2.2 Cluster-based MFD analysis using the whole sequence

For the statistical analysis of the MFD, we follow the procedure described in Methods. Table 1 and Fig. 3 indicate differences and similarities in the MFD among the clusters. In particular, Table 1 suggests that C1, C2, and C3 have identical MFD shapes, but that the MFD of C1 and C2 are distinct from the ones of C4 and C5. There is a tendency that C1 differs from C2, although not statistically significant. Figure 3 provides more details about the MFD behavior in terms of the b-value as function of M_c. For instance, the largest clusters C1–C3 (red, blue, and green, respectively) have comparable b-values (~1.2) at their corresponding $M_c^{\text{Lilliefors}}$, but behave differently for increasing M_c: for $M_w \geq 3.0$, the b-value is much higher in C3 than in C1 or C2. The small-scale clusters C4

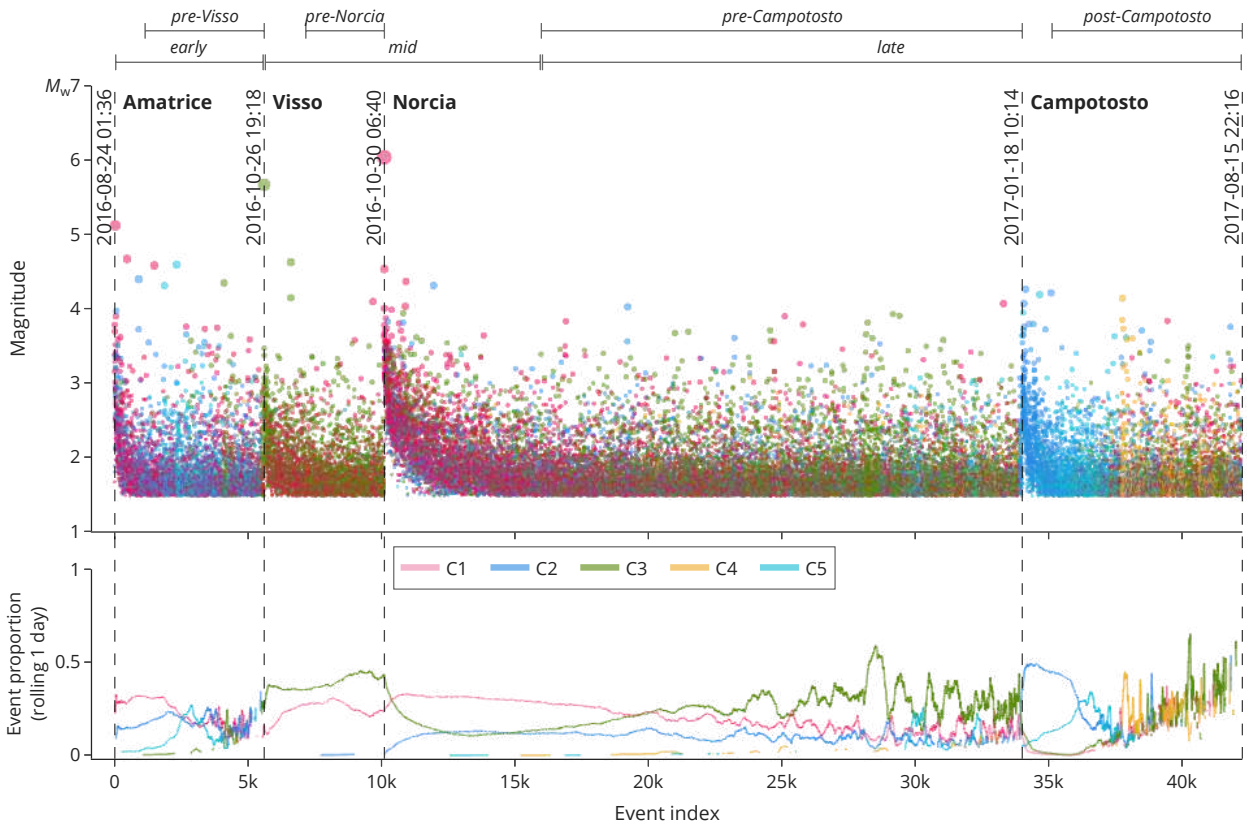

Figure 2: Temporal evolution of CI2016 seismicity colored by cluster association. Note that the x-axis represents the event index of all shown events (i. e., excluding unclustered events). The horizontal whiskers at the top indicate the periods of the temporal subsets. The bottom panel shows the event proportion of each cluster as fraction of the total events (including unclustered events) within a rolling window of the previous 24 hr.

Table 1: Pairwise comparison of the cumulative magnitude distribution of each cluster against the others.

	Cluster 1	Cluster 2	Cluster 3	Cluster 4	Cluster 5
Cluster 1		0.089	0.26	**2.2e-06**	**1.2e-06**
Cluster 2	0.089		0.59	**0.024**	**0.0084**
Cluster 3	0.26	0.59		0.49	0.36
Cluster 4	**2.2e-06**	**0.024**	0.49		0.51
Cluster 5	**1.2e-06**	**0.0084**	0.36	0.51	

p-values of two-sample Kolmogorov–Smirnov tests (see Methods). Statistically significant p-values are highlighted in bold.

and C5 (yellow and cyan, respectively) show the highest overall b-value. The Lilliefors p-value is useful to judge the reliability of the b-value; a p-value dropping below 0.1 indicates that the b-value for C1 and C3 below M_w2.0 does not relate to a persistent exponentiality with M_c, which can have several reasons (see Supplementary Note 2.2) and necessitates an inspection of the MFD in individual periods, as done in the following subsection.

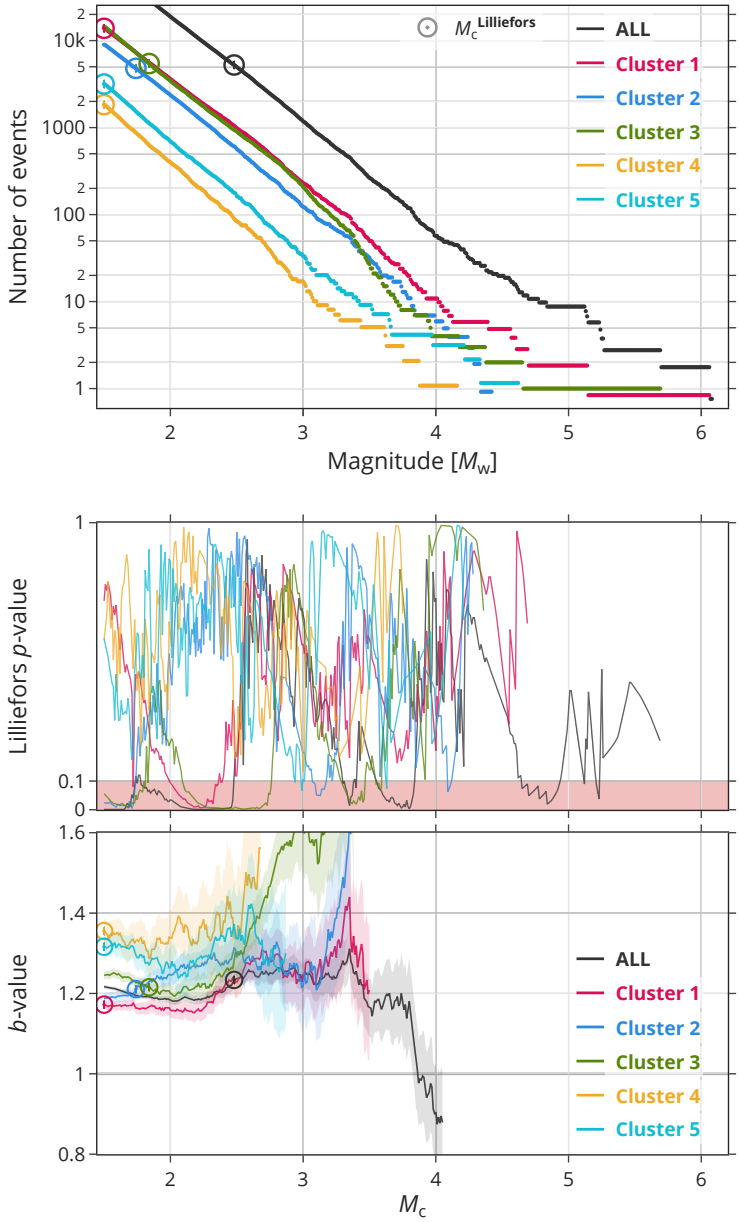

Figure 3: Magnitude statistics for all extracted data (black) and individual clusters (see legend). The top panel shows the data in terms of their magnitude–frequency distribution (MFD). Note that a tiny value is added to each MFD (between -0.1 and 0.1) to avoid visual overlaps at large magnitudes. The middle and bottom panel show, as a function of lower magnitude cutoff, or magnitude of completeness, M_c, the Lilliefors p-value (assuming an exponential distribution as null hypothesis) and the b-value (the slope of the fitted Gutenberg–Richter relation), respectively (see Methods). The $M_c^{\text{Lilliefors}}$ estimates are indicated for each cluster in the top and bottom panels with a circle marker. Supplementary Fig. S3 shows the same analysis using local magnitudes.

For the sake of completeness, we repeated the analysis using local magnitudes, M_L (see Supplementary Fig. S3), which introduces a different MFD behavior for the individual clusters due to a narrower exponential range (see Supplementary Note 2.3).

Table 2: Pairwise MFD comparison of temporal subsets. Like Table 1, but for three periods of Cluster 1, 2, and 3 that exclude short-term incompleteness (STAI).

	Cluster 1			Cluster 2			Cluster 3		
	(pre-V.)	(pre-N.)	(pre-C.)	(pre-V.)	(pre-N.)	(pre-C.)	(pre-V.)	(pre-N.)	(pre-C.)
C1 (pre-Visso)		**0.0037**	0.33	0.59	0.73	**0.03**	**2.1e-05**	0.86	0.79
C1 (pre-Norcia)	**0.0037**		0.23	**0.01**	0.73	**0.044**	**1.3e-09**	**0.0056**	0.052
C1 (pre-Campotosto)	0.33	0.23		0.52	0.42	0.21	**6e-06**	0.62	**0.013**
C2 (pre-Visso)	0.59	**0.01**	0.52		0.78	0.28	**2.5e-06**	0.51	0.067
C2 (pre-Norcia)	0.74	0.72	0.42	0.79		0.51	0.093	0.43	0.26
C2 (pre-Campotosto)	**0.03**	**0.044**	0.21	0.28	0.5		**7.6e-08**	**0.0087**	**0.018**
C3 (pre-Visso)	**2.1e-05**	**1.3e-09**	**5.8e-06**	**2.5e-06**	0.093	**7.6e-08**		**3.1e-06**	**0.012**
C3 (pre-Norcia)	0.86	**0.0056**	0.62	0.51	0.42	**0.0087**	**3.2e-06**		0.098
C3 (pre-Campotosto)	0.79	0.052	**0.013**	0.068	0.26	**0.018**	**0.012**	0.099	

2.3 Cluster-based MFD analysis using temporal subsets

We extend the spatial analysis by a temporal component using three periods that exclude the short-term aftershock incompleteness (STAI) between the main events, namely 'pre-Visso', 'pre-Norcia', and 'pre-Campotosto' (see Methods). Table 2 provides a more granular breakdown of MFD variations above $M_c^{\text{Lilliefors}}$ than Table 1, also temporally within the same cluster. For instance, in C1, only pre-Visso and pre-Norcia are distinct; in C2, no period is distinct, and in C3, pre-Visso is distinct from the other two periods. The MFD in pre-Campotosto is never distinct in any cluster. Comparisons among clusters for the same temporal period show no significant differences between C1 and C2, but when comparing C1 or C2 to C3. (Note that the sample size of C2 in pre-Norcia is very small (26 events), which reduces the power of the KS test to detect potential differences for pairs that include this subset.) The most unique subset is C3 during pre-Visso, which differs from almost all other subsets. Of all 36 pairs, 15 (42 %) are significantly different.

Further investigating the MFDs in terms of a M_c-dependent b-value (Figs. 4 and 5) provides a more nuanced discrimination. The most remarkable observation is that the b-value in C1 is highest before the Norcia mainshock—it has increased after the Visso event from 1.4 to 1.6. After the Norcia mainshock, the b-value remained at a high level (1.5 in the pre-Campotosto period). In C2, the b-value remained high at ∼1.45 both before the Visso and after the Norcia mainshock. (This cluster does not have enough events in the pre-Norcia period to estimate a b-value.) In C3, which contains the Visso event, the b-value increased from 1.0 in pre-Visso to 1.4 in pre-Norcia, at which level it stayed also after the Norcia mainshock.

Fig. 4 facilitates a temporal comparison of the MFD among the clusters. In pre-Visso, the b-value is similar in C1 and C2 at around 1.4, and much lower in C3 (1.0). Prior to the Norcia mainshock, the b-value increased both in C1 and C3 (to 1.4−1.6); C2 does not provide enough data. After the Norcia mainshock (i. e., pre-Campotosto), the b-value remains elevated in C1–C3 (1.3−1.5) and C1 and C2 have similar b-values again. After the Campotosto events (see Supplementary Fig. S8, 'post-Campotosto'), the b-value still remains elevated in C1–C3 (1.4−1.5).

For the sake of completeness, we repeated the analysis using M_L (see Supplementary Figs. S4, S5,

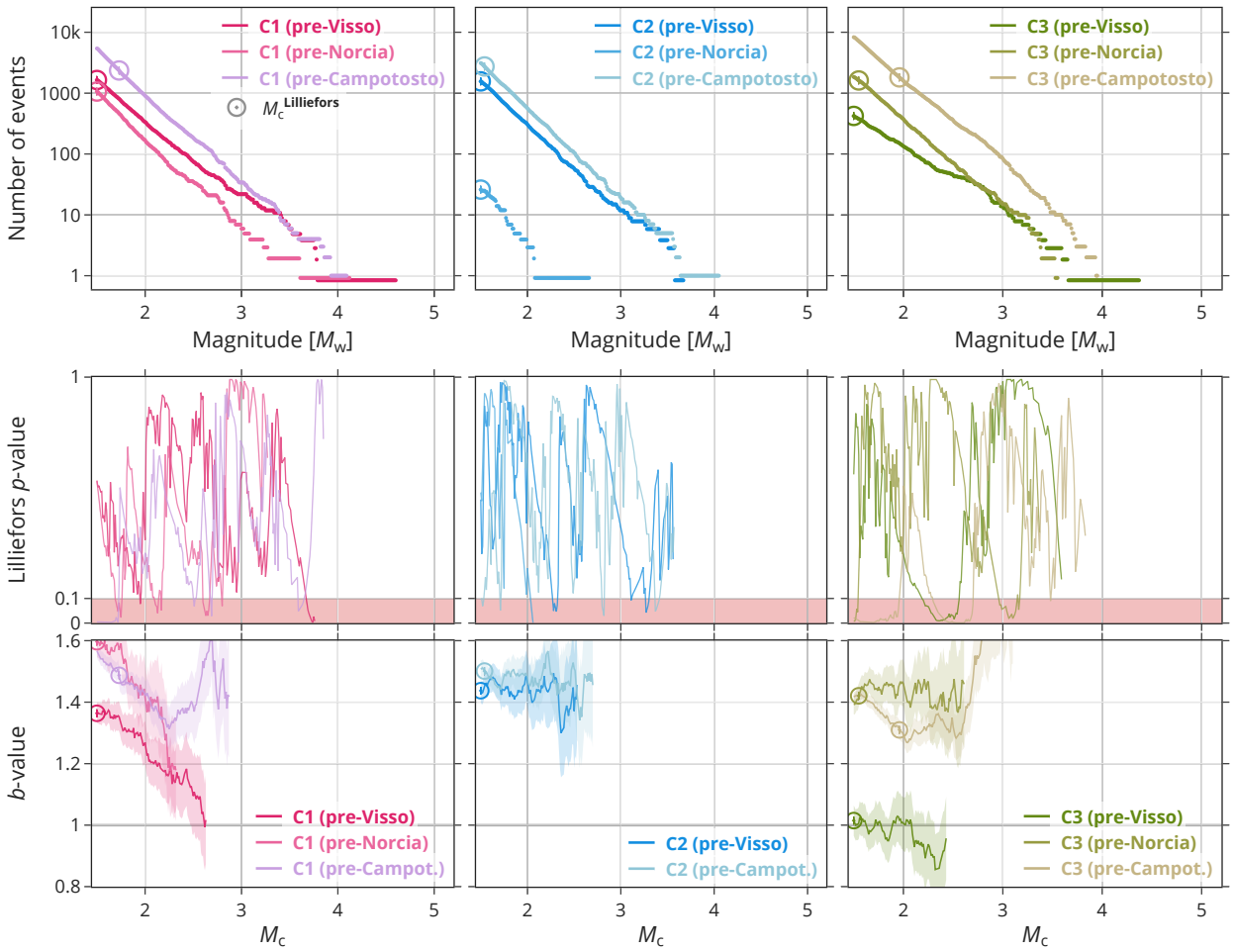

Figure 4: Magnitude statistics in three individual periods of Cluster 1 (left), Cluster 2 (center), and Cluster 3 (right). Like Fig. 3, the top panels show clusters in terms of their magnitude–frequency distribution; the middle and bottom panels show the Lilliefors p-value and b-value as function of M_c, respectively. Supplementary Fig. S4 shows the same analysis using local magnitudes. Supplementary Figs. S7 and S8 compares the periods shown here with periods that include STAI.

and Supplementary Note 2.3), which reproduces our main findings qualitatively with comparable *relative* b-value changes, albeit the b-value behaves differently as function of M_c owing to the scale change. For a comparison using temporal periods that include STAI, see Supplementary Note 2.4 and Supplementary Figs. S6–S8.

3 Discussion

We found that individual earthquake clusters that represent the most active zones of a complex sequence are characterized by a significantly different MFD behavior. In particular, the MFD can experience variations as temporal changes and spatial differences, or remain identical within one cluster throughout the sequence. This observed MFD variability is likely due to fine-scale heterogeneity and complexity of the tectonic structures that were activated in this sequence. In

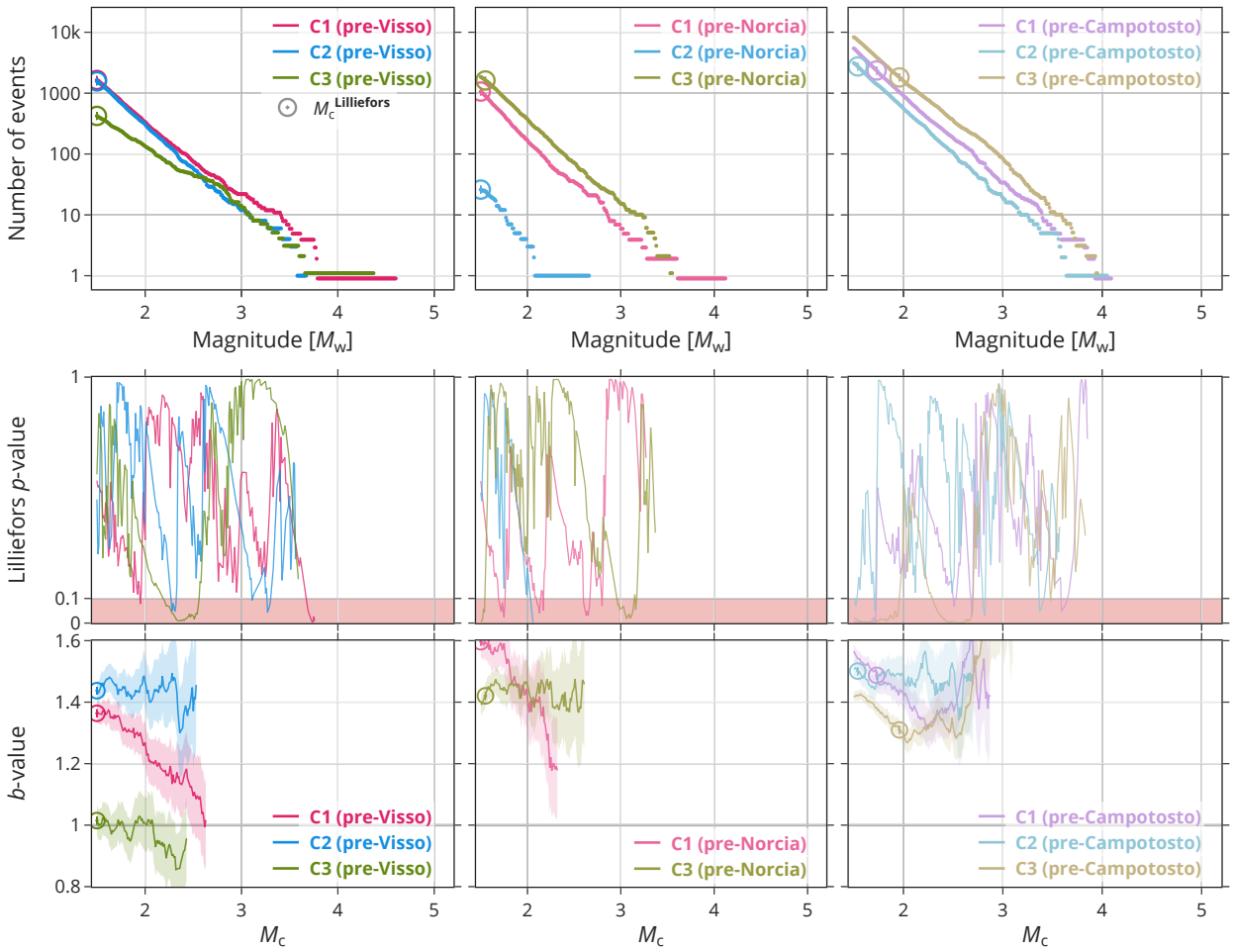

Figure 5: Reordering the magnitude statistics of Fig. 4 temporally by periods: 'pre-Visso' (left), 'pre-Norcia' (center), and 'pre-Campotosto' (right). Like Figs. 3 and 4, the top panels show clusters in terms of their magnitude–frequency distribution; the middle and bottom panels show the Lilliefors p-value and b-value as function of M_c. Supplementary Fig. S5 shows the same analysis using local magnitudes.

the following, we first discuss the observed temporal behavior, followed by a discussion of spatial differences and similarities, an interpretation of our findings, and a summary.

Regarding temporal changes, the most striking observation is the progressive b-value increase in the structure where the strongest earthquake eventually occurred (C1). Apparently, a high b-value did not prevent the nucleation of a large rupture in this structure. This resolved behavior differs from the general observation that the b-value decreases prior to large earthquakes [e. g., *Suyehiro et al.* 1964; *Nanjo et al.* 2012; *Tormann et al.* 2015; *Gulia et al.* 2016; *Gulia and Wiemer* 2019], albeit similar observations to ours do exist [e. g., *Nanjo and Yoshida* 2017]. The increasing b-value in C1 after the Visso event highlights that activity in one cluster may influence the MFD in another one. After the Visso event, the b-value also increased in its own cluster (C3), which corroborates that large events may influence the MFD in their surrounding as already found by [*Gulia et al.* 2018]. The later Norcia mainshock, however, did not alter the MFD in the three main clusters further and the b-value remained high—also after the Campotosto events. This stagnating b-value highlights that the MFD eventually became insensitive to strong seismicity even though it had

experienced significant temporal variations in the same structures earlier. This ambivalent character is compounded by the MFD behavior in C2, where the MFD locally remained constant throughout the sequence and apparently unaffected by surrounding seismicity.

When comparing clusters spatially regarding the whole sequence, we found differences in the MFD between the largest clusters (C1 and C2) and the smaller ones (C4 and C5). The former have overall lower b-value estimates, which are due to the stronger influence of STAI as a result of their proximity to larger events. In fact, the b-value estimate can be much lower in periods that include STAI (see Supplementary Note 2.4 and Supplementary Figs. S7–S9). In each of these time periods, we found spatial MFD differences among the largest clusters (C3 differing from C1 and C2). Simultaneously, MFD similarities coexisted among these clusters (C1 and C2), although we do not have evidence for every time period, such as for pre-Norcia when C2 only provides few samples. C1 and C2 have in common that they represent the majority of seismicity in the subhorizontal structure at depth (its northern and southern extension, respectively). Their MFD differs from C3 in each individual period and tend toward a higher b-value, which means that this subhorizontal structure is not only tectonically distinct from the shallower normal faults (see Introduction), but also in terms of the MFD.

Although our study focuses on raising awareness of appropriately resolving MFD and b-value variations, we briefly speculate about the underlying causes for our most remarkable observations in this sequence. The marked MFD variability among the clusters over time likely reflects a heterogeneous stress field and/or a complex fault geometry with significant contributions from the subhorizontal detachment. Moreover, a complex rupture process is suggested by the fact that only some of the main events belong to clusters—a result of the different event densities surrounding these hypocenters. The generally higher b-value in the subhorizontal structure could be caused by the structure's reduced capacity to accumulate stress (i. e., low differential stress). Instead of accumulating stress, it preferentially transfers stress to the shallow fault system, favoring its unlocking [*Vuan et al.* 2017]. Moreover, this subhorizontal thrust is known to release microearthquakes quasi-continuously along its entire length [*Chiaraluce* 2012; *Chiaraluce et al.* 2017], occasionally in minor sequences [*Ciaccio* 2016; *Moschella et al.* 2021], but not hosting larger earthquakes (which should have an extensional mechanism). The very high b-value prior and close to the hypocenter of the Norcia mainshock could be explained with (i) the generally high b-value in the subhorizontal structure, because C1's pre-Norcia seismicity occurred within its north-eastern extension (see Supplementary Fig. S10), whereas its pre-Visso seismicity was located in a shallower part; and (ii) a consequence of the previous two main events (Amatrice and Visso) and their aftershocks generally reducing the differential stress in its surrounding by releasing built-up strain, i. e., stored energy, on the normal faults. Note that the Norcia mainshock nucleated in between the pre-Norcia and the pre-Visso subset of C1 (i. e., the aftershock zones of Amatrice and Visso, respectively, see also *Improta et al.* [2019]), which is consistent with observations that large events tend to nucleate at the rim of seismic clouds [van der *Elst and Shaw* 2015; *Stallone and Marzocchi* 2019] and the cascading stress transfer hypothesis [e. g., *Ellsworth and Bulut* 2018; *Gomberg* 2018].

In summary, our study demonstrated that the spatiotemporal isolation of seismicity clusters resolves a distinct MFD behavior among the most active zones over time, including influences between them. We therefore argue that the MFD highly depends on the observed substructure. Since the most active structures in turn influence the overall MFD behavior of a sequence, a consideration

of the activity in individual structures allows us to decompose and analyze the most important contributions of a complex sequence. Our findings point to the problem of choosing an appropriate spatiotemporal scale to resolve the b-value, challenging existing approaches: A too large scale merges potentially different MFD behavior of individual structures and a too fine resolution obscures the tectonic relation and reduces the statistical robustness. The cluster-based approach presented here uses the distribution of the seismicity itself to choose a scale that is physically meaningful and provides robust statistics. Moreover, a spatial scale inferred from a cluster analysis may serve as an appropriate reference volume for the background b-value—provided that the (moment) magnitude estimates are consistent. In Supplementary Note 2 we discuss several more factors and choices that influence and potentially bias the b-value estimate, most importantly related to the sample size, exponentiality, STAI, and magnitude scale. Those aspects are not always carefully addressed when performing b-value analyses. We highlight that the absolute b-value has little meaning not only due to its dependence on the magnitude scale (see Supplementary Note 2.3), but also on the particular conversion relation (see Supplementary Note 2.5 and Supplementary Fig. S9). We hypothesize that a complex and distinct MFD behavior is not unique to the CI2016 sequence, but likely occurs in other regions and sequences. Our method may be beneficial in studying the peculiarities of spatiotemporal MFD variability and improving our understanding of the processes that influence seismicity. Even if the physical mechanisms remain hidden, recognizing that the MFD behaves complex potentially improves spatiotemporal forecast performance. Our approach based on an established clustering algorithm may also help to reduce the amount of expert judgment and subjective choices in MFD analysis, which could facilitate an application in real-time. Future work may focus on a refined identification of spatiotemporal clusters to improve MFD and b-value analysis, possibly by not relying solely on event density.

4 Methods

4.1 High-resolution earthquake catalog of the sequence

We use the high-resolution catalog of *Tan et al.* [2021], which spans from 2016-08-15 to 2017-08-15, and extracted a spatial subset as follows: depth < 12 km; UTM easting: 330–370 km (about longitude 12.94–13.40); UTM northing: 4690–4790 km (about latitude 42.34–43.25). Only events with moment magnitudes $M_\mathrm{w} \geq 1.5$ were used, totaling 76 055 events. The M_w contained in the catalog were converted from local magnitudes, M_L, using the polynomial fit of *Grünthal et al.* [2009], an average European scaling relation based on catalogs of different seismological agencies with most events having $M_\mathrm{L} > 1.5$ and $M_\mathrm{w} \gtrsim 1.5$. For magnitudes of large events to match, *Tan et al.* [2021] calibrated its constant (0.53) to 0.817 (i. e., +0.287).

4.2 Creating spatial earthquake clusters and temporal subclusters

Seismicity was grouped spatially into clusters using DBSCAN [Density-Based Spatial Clustering of Applications with Noise, *Ester et al.* 1996], which groups points based on how closely they are packed together. Points that lie in low-density regions are left as outliers. Because the

horizontal extension of the CI2016 sequence is several times larger than the vertical extension, density-connected clouds of hypocenters preferentially extend in horizontal directions. To improve the clustering analysis for such an anisotropic case, data dimensions are usually rescaled beforehand. We therefore rescale the hypocenter coordinates to a uniform extent in each direction, i. e., rescaled into a cube. This procedure increases the local point density in horizontal planes, which facilitates identifying hypocenter clusters with horizontally elongated shapes (see Supplementary Fig. S1). We then applied DBSCAN with the following parameters: $\epsilon = 0.40$, the neighborhood radius and $Z = 200$, the minimum number of points required to form a dense region. This configuration yielded nine clusters, from which we selected the five largest (C1–5, descending by size) and labeled the remaining events as 'unclustered'. Their spatial distribution is shown in Fig. 1 and the data provided as Supplementary Data.

To enable a temporal analysis, each of the largest clusters C1–C3 was divided into three periods (see indicators in Fig. 2):

- '*early*': events before the Visso event;
- '*mid*': events from the Visso event until two days after the Norcia mainshock;
- '*late*': the rest.

Note that there is too few data in C4 and C5 to benefit from the division.

As illustrated in Supplementary Fig. S6, these periods are affected by short-term aftershock incompleteness [STAI, *Kagan* 2004; *Helmstetter et al.* 2006; *Hainzl* 2016; de *Arcangelis et al.* 2018, see also Supplementary Note 2.4]. Supplementary Fig. S6 makes use of equalized plot scales as suggested by *Agnew* [2015] and overlays the event density as suggested by W. Ellsworth (pers. comm., 2021). In this way, Supplementary Fig. S6 informs us about the STAI duration after each main event, leading us to exclude STAI by using a temporal subset of each period for C1, C2, and C3 (see indicators at the top of Fig. 2):

- '*pre-Visso*': like *early*, but excluding the first 0.8 days after the Amatrice event;
- '*pre-Norcia*': like *mid*, but excluding the first 0.6 days after the Visso event and 2.0 days after the Norcia mainshock;
- '*pre-Campotosto*': like *late*, but before the Campotosto event;
- '*post-Campotosto*': like *late*, but after the Campotosto event excluding the first 0.4 days.

4.3 Earthquake statistics

The clusters and their temporal subsets are investigated in terms of their MFD. To quantify MFD differences, we calculate the b-value as function of M_c. The b-value is determined using the bias-free maximum likelihood estimation of *Tinti and Mulargia* [1987] and *Marzocchi and Sandri* [2003] for sample sizes $N \geq 50$. The b-value requires an exponential distribution of the magnitude above M_c to be physically meaningful [*Marzocchi et al.* 2020]. To assess the exponentiality of the MFD, we apply the Lilliefors test [*Marzocchi et al.* 2020; *Herrmann and Marzocchi* 2021], using the implementation of *Herrmann and Marzocchi* [2020], and obtain a p-value as function of M_c,

which expresses the probability to observe the MFD assuming that the exponential distribution is the underlying distribution. For a significance level of $\alpha = 0.1$, we derive the lowest magnitude level for which the MFD can be considered exponential, referred to as $M_c^{\text{Lilliefors}}$. We always refer to the b-value at $M_c^{\text{Lilliefors}}$.

As an alternative to quantify MFD differences, we use the two-sample Kolmogorov–Smirnov (KS) test and compare the MFD of clusters or their temporal subsets pairwise. For each pair, the largest $M_c^{\text{Lilliefors}}$ is used as lower magnitude cutoff. The KS test returns a p-value as a measure for the strength of evidence against the null hypothesis that the two MFDs come from the same parent distribution. We interpret a p-value < 0.05 as a statistically significant difference.

We do not explore whether the MFD can be characterized by a tapered GR distribution, and therefore neglect variations of the corner magnitude, e. g., due to released energy close to faults [*Spassiani and Marzocchi* 2021]. While the b-value correlates with the largest magnitude [*Marzocchi et al.* 2020], the KS test has reduced sensitivity toward the tails of the distributions. We assume that distinct b-values or significant p-values reflect differences or changes of the entire exponential part of the MFD.

4.4 Prior seismicity

The high-resolution catalog of *Tan et al.* [2021] only contains 15 events with $M_w \geq 1.5$ before the start of the sequence (i. e., before the Amatrice event). For a comparison of seismicity during the sequence with prior seismicity, we have initially considered HORUS [*Lolli et al.* 2020, `horus.bo.ingv.it`] as a temporally extensive catalog that provides M_w magnitudes. Those magnitudes were converted from M_L using a magnitude regression that differs from the conversion relation used in the CI2016 catalog of *Tan et al.* [2021]. In fact, a comparative MFD analysis for CI2016 seismicity shows that the b-value differs considerably between both catalogs (0.2 units at $M_c^{\text{Lilliefors}}$, see Supplementary Note 2.5 and Supplementary Fig. S9). Therefore, the two M_w scales are not consistent with each other. This inconsistency does not allow a reliable comparison of the b-value among these two catalogs (e. g., against a reference "background" b-value based on HORUS). We therefore did not consider HORUS data in our MFD analyses.

Data availability

All data generated or analyzed during this study are included in this article (and its supplementary information files).

Acknowledgments

This study was supported by the *'Real-time Earthquake Risk Reduction for a Resilient Europe'* (RISE) project, funded by the European Union's *Horizon 2020* research and innovation program

(Grant Agreement No. 821115). We thank the creators and maintainers of `plotly`'s Python graphing library (`www.plotly.com/python`).

Author contributions

M.H. performed the statistical analyses, created the figures, and wrote the manuscript. E.P. performed the clustering analysis and reviewed the manuscript. W.M. lead the project and reviewed the manuscript. All authors designed the study and discussed the results.

References

Agnew, D. C. (2015). "Equalized Plot Scales for Exploring Seismicity Data". In: *Seismological Research Letters* 86.5, pp. 1412–1423. DOI: 10.1785/0220150054.

Bachmann, C. E., S. Wiemer, B. P. Goertz-Allmann, and J. Wössner (2012). "Influence of pore-pressure on the event-size distribution of induced earthquakes". In: *Geophysical Research Letters* 39.9. DOI: 10.1029/2012GL051480.

Beroza, G. C., M. Segou, and S. Mostafa Mousavi (2021). "Machine learning and earthquake forecasting—next steps". In: *Nature Communications* 12.1, p. 4761. DOI: 10.1038/s41467-021-24952-6.

Chiaraluce, L. (2012). "Unravelling the complexity of Apenninic extensional fault systems: A review of the 2009 L'Aquila earthquake (Central Apennines, Italy)". In: *Journal of Structural Geology* 42, pp. 2–18. DOI: 10.1016/j.jsg.2012.06.007.

Chiaraluce, L. *et al.* (2017). "The 2016 Central Italy Seismic Sequence: A First Look at the Mainshocks, Aftershocks, and Source Models". In: *Seismological Research Letters* 88.3, pp. 757–771. DOI: 10.1785/0220160221.

Ciaccio, M. G. (2016). "Instrumental seismicity of the Amatrice earthquake epicentral area: A review". In: *Annals of Geophysics* 59.FASTTRACK5, pp. 1–8. DOI: 10.4401/ag-7283.

Dascher-Cousineau, K., T. Lay, and E. E. Brodsky (2021). "Reply to "Comment on 'Two Foreshock Sequences Post Gulia and Wiemer (2019)' by Kelian Dascher-Cousineau, Thorne Lay, and Emily E. Brodsky" by Laura Gulia and Stefan Wiemer". In: *Seismological Research Letters* 92.5, pp. 3259–3264. DOI: 10.1785/0220210059.

De Luca, G., M. Cattaneo, G. Monachesi, and A. Amato (2009). "Seismicity in central and Northern Apennines integrating the Italian national and regional networks". In: *Tectonophysics*. DOI: 10.1016/j.tecto.2008.11.032.

De Arcangelis, L., C. Godano, and E. Lippiello (2018). "The Overlap of Aftershock Coda Waves and Short-Term Postseismic Forecasting". In: *Journal of Geophysical Research: Solid Earth* 123.7, pp. 5661–5674. DOI: 10.1029/2018JB015518.

Dublanchet, P. (2020). "Stress-Dependent b Value Variations in a Heterogeneous Rate-and-State Fault Model". In: *Geophysical Research Letters*. DOI: 10.1029/2020GL087434.

Ellsworth, W. L. and F. Bulut (2018). "Nucleation of the 1999 Izmit earthquake by a triggered cascade of foreshocks". In: *Nature Geoscience* 0. DOI: 10.1038/s41561-018-0145-1.

Ester, M., H.-P. Kriegel, J. Sander, and X. Xu (1996). "A Density-Based Algorithm for Discovering Clusters in Large Spatial Databases with Noise". In: *Proceedings of the 2nd International Conference on Knowledge Discovery and Data Mining (KDD-96)*. AAAI Press, pp. 226–231.

García-Hernández, R., L. D'Auria, J. Barrancos, G. D. Padilla, and N. M. Pérez (2021). "Multiscale Temporal and Spatial Estimation of the b-Value". In: *Seismological Research Letters* 92.6, pp. 3712–3724. DOI: 10.1785/0220200388.

Ghosh, A., A. V. Newman, A. M. Thomas, and G. T. Farmer (2008). "Interface locking along the subduction megathrust from b -value mapping near Nicoya Peninsula, Costa Rica". In: *Geophysical Research Letters* 35.1, p. L01301. DOI: 10.1029/2007GL031617.

Goebel, T. H., G. Kwiatek, T. W. Becker, E. E. Brodsky, and G. Dresen (2017). "What allows seismic events to grow big?: Insights from b-value and fault roughness analysis in laboratory stick-slip experiments". In: *Geology* 45.9, pp. 815–818. DOI: 10.1130/G39147.1.

Gomberg, J. (2018). "Unsettled earthquake nucleation". In: *Nature Geoscience* 11.7, pp. 463–464. DOI: 10.1038/s41561-018-0149-x.

Grünthal, G., R. Wahlström, and D. Stromeyer (2009). "The unified catalogue of earthquakes in central, northern, and northwestern Europe (CENEC)—updated and expanded to the last millennium". In: *Journal of Seismology* 13.4, pp. 517–541. DOI: 10.1007/s10950-008-9144-9.

Gulia, L., A. P. Rinaldi, T. Tormann, G. Vannucci, B. Enescu, and S. Wiemer (2018). "The Effect of a Mainshock on the Size Distribution of the Aftershocks". In: *Geophysical Research Letters* 45.24, pp. 13, 277–13, 287. DOI: 10.1029/2018GL080619.

Gulia, L., T. Tormann, S. Wiemer, M. Herrmann, and S. Seif (2016). "Short-term probabilistic earthquake risk assessment considering time-dependent b values". In: *Geophysical Research Letters* 43.3, pp. 1100–1108. DOI: 10.1002/2015GL066686.

Gulia, L. and S. Wiemer (2019). "Real-time discrimination of earthquake foreshocks and aftershocks". In: *Nature* 574.7777, pp. 193–199. DOI: 10.1038/s41586-019-1606-4.

Gulia, L. and S. Wiemer (2021). "Comment on "Two Foreshock Sequences Post Gulia and Wiemer (2019)" by Kelian Dascher-Cousineau, Thorne Lay, and Emily E. Brodsky". In: *Seismological Research Letters* 92.5, pp. 3251–3258. DOI: 10.1785/0220200428.

Hainzl, S. (2016). "Apparent triggering function of aftershocks resulting from rate-dependent incompleteness of earthquake catalogs". In: *Journal of Geophysical Research: Solid Earth* 121.9, pp. 6499–6509. DOI: 10.1002/2016JB013319.

Hainzl, S. and T. Fischer (2002). "Indications for a successively triggered rupture growth underlying the 2000 earthquake swarm in Vogtland/NW Bohemia". In: *Journal of Geophysical Research: Solid Earth* 107.B12, ESE 5–1–ESE 5–9. DOI: 10.1029/2002JB001865.

Helmstetter, A., Y. Y. Kagan, and D. D. Jackson (2006). "Comparison of short-term and time-dependent earthquake forecast models for southern California". In: *Bulletin of the Seismological Society of America* 96.1, pp. 90–106. DOI: 10.1785/0120050067.

Herrmann, M. and W. Marzocchi (2020). *Mc-Lilliefors: A completeness magnitude that complies with the exponential-like Gutenberg-Richter relation*. DOI: 10.5281/zenodo.4162497.

Herrmann, M. and W. Marzocchi (2021). "Inconsistencies and Lurking Pitfalls in the Magnitude–Frequency Distribution of High-Resolution Earthquake Catalogs". In: *Seismological Research Letters* 92.2A, pp. 909–922. DOI: 10.1785/0220200337.

Igonin, N., M. Zecevic, and D. W. Eaton (2018). "Bilinear Magnitude-Frequency Distributions and Characteristic Earthquakes During Hydraulic Fracturing". In: *Geophysical Research Letters*. DOI: 10.1029/2018GL079746.

Improta, L. *et al.* (2019). "Multi-segment rupture of the 2016 Amatrice-Visso-Norcia seismic sequence (central Italy) constrained by the first high-quality catalog of Early Aftershocks". In: *Scientific Reports* 9.1, p. 6921. DOI: 10.1038/s41598-019-43393-2.

El-Isa, Z. H. and D. W. Eaton (2014). "Spatiotemporal variations in the b-value of earthquake magnitude-frequency distributions: Classification and causes". In: *Tectonophysics* 615-616, pp. 1–11. DOI: 10.1016/j.tecto.2013.12.001.

Jordan, T. H. *et al.* (2011). "Operational earthquake forecasting: State of knowledge and guidelines for utilization". In: *Annals of Geophysics* 54.4. DOI: 10.4401/ag-5350.

Kagan, Y. Y. (2002). "Seismic moment distribution revisited: I. Statistical results". In: *Geophysical Journal International* 148.3, pp. 520–541. DOI: 10.1046/j.1365-246x.2002.01594.x.

Kagan, Y. Y. (2004). "Short-Term Properties of Earthquake Catalogs and Models of Earthquake Source". In: *Bulletin of the Seismological Society of America* 94.4, pp. 1207–1228. DOI: 10.1785/012003098.

Lolli, B., D. Randazzo, G. Vannucci, and P. Gasperini (2020). "The Homogenized Instrumental Seismic Catalog (HORUS) of Italy from 1960 to Present". In: *Seismological Research Letters* 91.6, pp. 3208–3222. DOI: 10.1785/0220200148.

Marzocchi, W. and L. Sandri (2003). "A review and new insights on the estimation of the b-value and its uncertainty". In: *Annals of geophysics* 46.December, pp. 1271–1282. DOI: 10.4401/ag-3472.

Marzocchi, W., I. Spassiani, A. Stallone, and M. Taroni (2020). "How to be fooled searching for significant variations of the b-value". In: *Geophysical Journal International* 220.3, pp. 1845–1856. DOI: 10.1093/gji/ggz541.

Michele, M., L. Chiaraluce, R. Di Stefano, and F. Waldhauser (2020). "Fine-Scale Structure of the 2016–2017 Central Italy Seismic Sequence From Data Recorded at the Italian National Network". In: *Journal of Geophysical Research: Solid Earth* 125.4. DOI: 10.1029/2019JB018440.

Michele, M. *et al.* (2016). "The Amatrice 2016 seismic sequence: a preliminary look at the mainshock and aftershocks distribution". In: *Annals of Geophysics* 59.Fast Track 5, pp. 1–8. DOI: 10.4401/ag-7227.

Mogi, K. (1962). "Magnitude-Frequency Relation for Elastic Shocks Accompanying Fractures of Various Materials and Some Related Problems in Earthquakes (2nd Paper)". In: *Bulletin of the Earthquake Research Institute* 40.4, pp. 831–853. DOI: 10.15083/0000033759.

Montuori, C. A., M. Murru, and G. Falcone (2016). "Spatial variation of the b-value observed for the periods preceding and following the 24 August 2016, Amatrice earthquake (ML6.0) (central Italy)". In: *Annals of Geophysics* 59.FastTrack5. DOI: 10.4401/ag-7273.

Moschella, M., M. G. Ciaccio, and D. Latorre (2021). "Minor earthquake sequences in the Amatrice-Norcia epicentral area (Central Italy)". In: *Tectonophysics* 809.September 2020, p. 228858. DOI: 10.1016/j.tecto.2021.228858.

Nanjo, K. Z., N. Hirata, K. Obara, and K. Kasahara (2012). "Decade-scale decrease in b value prior to the M 9-class 2011 Tohoku and 2004 Sumatra quakes". In: *Geophysical Research Letters* 39.20, 2012GL052997. DOI: 10.1029/2012GL052997.

Nanjo, K. Z. and A. Yoshida (2017). "Anomalous decrease in relatively large shocks and increase in the p and b values preceding the April 16, 2016, M7.3 earthquake in Kumamoto, Japan". In: *Earth, Planets and Space* 69.1, p. 13. DOI: 10.1186/s40623-017-0598-2.

Nava, F. A., V. H. Márquez-Ramírez, F. R. Zúñiga, L. Ávila-Barrientos, and C. B. Quinteros (2016). *Gutenberg–Richter b-value maximum likelihood estimation and sample size*. DOI: 10.1007/s10950-016-9589-1.

Passarelli, L. *et al.* (2015). "Aseismic transient driving the swarm-like seismic sequence in the Pollino range, Southern Italy". In: *Geophysical Journal International* 201.3, pp. 1553–1567. DOI: 10.1093/gji/ggv111.

Petruccelli, A., D. Schorlemmer, T. Tormann, A. P. Rinaldi, S. Wiemer, P. Gasperini, and G. Vannucci (2019). "The influence of faulting style on the size-distribution of global earthquakes". In: *Earth and Planetary Science Letters* 527, p. 115791. DOI: 10.1016/j.epsl.2019.115791.

Porreca, M. *et al.* (2020). "3D geological reconstruction of the M. Vettore seismogenic fault system (Central Apennines, Italy): Cross-cutting relationship with the M. Sibillini thrust". In: *Journal of Structural Geology* 131.March 2019, p. 103938. DOI: 10.1016/j.jsg.2019.103938.

Roberts, N. S., A. F. Bell, and I. G. Main (2016). "Mode switching in volcanic seismicity: El Hierro 2011-2013". In: *Geophysical Research Letters* 43.9, pp. 4288–4296. DOI: 10.1002/2016GL068809.

Scholz, C. H. (2015). "On the stress dependence of the earthquake b value". In: *Geophysical Research Letters* 42.5, pp. 1399–1402. DOI: 10.1002/2014GL062863.

Schorlemmer, D., S. Wiemer, and M. Wyss (2005). "Variations in earthquake-size distribution across different stress regimes." In: *Nature* 437.7058, pp. 539–42. DOI: 10.1038/nature04094.

Schorlemmer, D. *et al.* (2018). "The Collaboratory for the Study of Earthquake Predictability: Achievements and Priorities". In: *Seismological Research Letters* 89.4, pp. 1305–1313. DOI: 10.1785/0220180053.

Shelly, D. R., W. L. Ellsworth, and D. P. Hill (2016). "Fluid-faulting evolution in high definition: Connecting fault structure and frequency-magnitude variations during the 2014 Long Valley Caldera, California, earthquake swarm". In: *Journal of Geophysical Research: Solid Earth* 121.3, pp. 1776–1795. DOI: 10.1002/2015JB012719.

Sobiesiak, M., U. Meyer, S. Schmidt, H.-J. Götze, and C. M. Krawczyk (2007). "Asperity generating upper crustal sources revealed by b value and isostatic residual anomaly grids in the area of Antofagasta, Chile". In: *Journal of Geophysical Research* 112.B12, B12308. DOI: 10.1029/2006JB004796.

Spassiani, I. and W. Marzocchi (2021). "An energy-dependent earthquake moment–frequency distribution". In: *Bulletin of the Seismological Society of America* 111.2, pp. 762–774. DOI: 10.1785/012020190.

Stallone, A. and W. Marzocchi (2019). "Empirical evaluation of the magnitude-independence assumption". In: *Geophysical Journal International* 216.2, pp. 820–839. DOI: 10.1093/gji/ggy459.

Suyehiro, S., T. Asada, and M. Ohtake (1964). "Foreshocks and Aftershocks Accompanying a Perceptible Earthquake in Central Japan". In: *Papers in Meteorology and Geophysics* 15.1, pp. 71–88. DOI: 10.2467/mripapers1950.15.1_71.

Tan, Y. J. *et al.* (2021). "Machine-Learning-Based High-Resolution Earthquake Catalog Reveals How Complex Fault Structures Were Activated during the 2016–2017 Central Italy Sequence". In: *The Seismic Record* 1.1, pp. 11–19. DOI: 10.1785/0320210001.

Taroni, M., J. Zhuang, and W. Marzocchi (2021). "High-Definition Mapping of the Gutenberg–Richter b-Value and Its Relevance: A Case Study in Italy". In: *Seismological Research Letters* 92.6, pp. 3778–3784. DOI: 10.1785/0220210017.

Tinti, S. and F. Mulargia (1987). "Confidence intervals of b values for grouped magnitudes". In: *Bulletin of the Seismological Society of America* 77.6, pp. 2125–2134. URL: https://pubs.geoscienceworld.org/ssa/bssa/article/77/6/2125/119039.

Tondi, E., D. Jablonská, T. Volatili, M. Michele, S. Mazzoli, and P. P. Pierantoni (2020). "The Campotosto linkage fault zone between the 2009 and 2016 seismic sequences of central Italy: Implications for seismic hazard analysis". In: *GSA Bulletin* 133.7, pp. 1679–1694. DOI: 10.1130/B35788.1.

Tormann, T., B. Enescu, J. Woessner, and S. Wiemer (2015). "Randomness of megathrust earthquakes implied by rapid stress recovery after the Japan earthquake". In: *Nature Geoscience* 8.2, pp. 152–158. DOI: 10.1038/ngeo2343.

Tormann, T., S. Wiemer, S. Metzger, A. J. Michael, and J. L. Hardebeck (2013). "Size distribution of Parkfield's microearthquakes reflects changes in surface creep rate". In: *Geophysical Journal International* 193.3, pp. 1474–1478. DOI: 10.1093/gji/ggt093.

Van der Elst, N. J. and B. E. Shaw (2015). "Larger aftershocks happen farther away: Nonseparability of magnitude and spatial distributions of aftershocks". In: *Geophysical Research Letters* 42.14, pp. 5771–5778. DOI: 10.1002/2015GL064734.

Vuan, A., M. Sugan, L. Chiaraluce, and R. Di Stefano (2017). "Loading Rate Variations Along a Midcrustal Shear Zone Preceding the M w 6.0 Earthquake of 24 August 2016 in Central Italy". In: *Geophysical Research Letters* 44.24, pp. 12, 170–12, 180. DOI: 10.1002/2017GL076223.

Waldhauser, F., M. Michele, L. Chiaraluce, R. Di Stefano, and D. P. Schaff (2021). "Fault Planes, Fault Zone Structure and Detachment Fragmentation Resolved With High-Precision Aftershock Locations of the 2016–2017 Central Italy Sequence". In: *Geophysical Research Letters* 48.16, pp. 1–10. DOI: 10.1029/2021GL092918.

Wiemer, S. and M. Wyss (1997). "Mapping the frequency-magnitude distribution in asperities: An improved technique to calculate recurrence times?" In: *Journal of Geophysical Research: Solid Earth* 102.B7, pp. 15115–15128. DOI: 10.1029/97jb00726.

Wiemer, S. and M. Wyss (2002). "Mapping spatial variability of the frequency-magnitude distribution of earthquakes". In: *Advances in Geophysics*. Ed. by R. Dmowska and B. Saltzman. Vol. 45. Elsevier, pp. 259–302. DOI: 10.1016/S0065-2687(02)80007-3.

Wyss, M. (1973). "Towards a Physical Understanding of the Earthquake Frequency Distribution". In: *Geophysical Journal International* 31.4, pp. 341–359. DOI: 10.1111/j.1365-246X.1973.tb06506.x.

Zechar, J. D., D. Schorlemmer, M. Liukis, J. Yu, F. Euchner, P. J. Maechling, and T. H. Jordan (2010). "The Collaboratory for the Study of Earthquake Predictability perspective on computational earthquake science". In: *Concurrency and Computation: Practice and Experience* 22.12, pp. 1836–1847. DOI: 10.1002/cpe.1519.

Supplementary Files

This is a list of supplementary files associated with this preprint. Click to download.

- datasuppTan2021extractMw1.5withClusterID.zip
- supplementclean.pdf